Electronic Supplementary Material (ESI) for Nanoscale Horizons.

Supporting Information

Ultrafast free carrier dynamics in black phosphorus-molybdenum disulfide (BP/MoS_2) heterostructure

Zhonghui Nie,[a,b] Yuhan Wang,[a,b] Ziling Li,[c] Yue Sun,[a] Shuchao Qin,[a] Xiaoping Liu,[d] Edmond Turcu,[a] Yi Shi,[a] Rong Zhang,[a] Yu Ye,[c] Yongbing Xu, [*a] Giulio Cerullo[*e,f] and Fengqiu Wang[*a,b]

[a]*School of Electronic Science and Engineering, Nanjing University, Nanjing 210023, China*
[b]*Key Laboratory of Intelligent Optical Sensing and Manipulation, Ministry of Education, Nanjing University, Nanjing 210093, China*
[c]*Department of Physics, Peking University, Beijing 100871, China*
[d]*College of Engineering and Applied Sciences, Nanjing University, Nanjing 210093, China*
[e]*Dipartimento di Fisica, Politecnico di Milano, Piazza Leonardo da Vinci 32, I-20133 Milano, Italy*
[f]*Istituto di Fotonica e Nanotecnologie (IFN), CNR, Piazza Leonardo da Vinci 32, I-20133 Milano, Italy.*

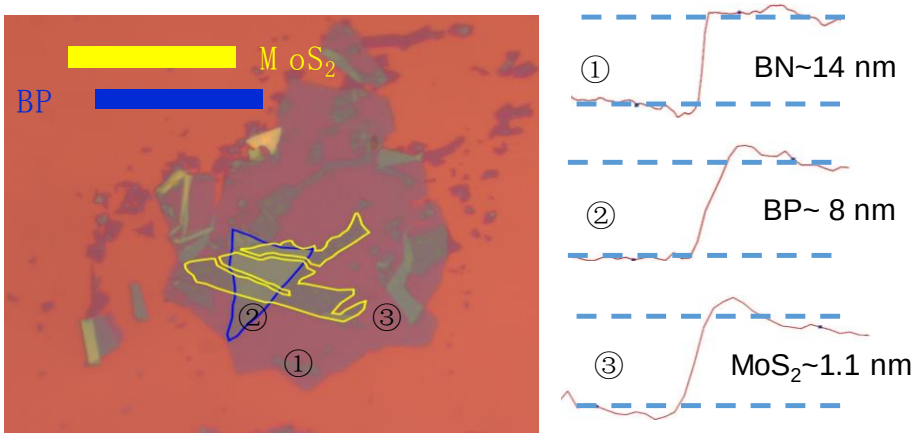

Figure S1. Atomic force microscopy (AFM) characterization of different components in BP/MoS_2 heterostructure.

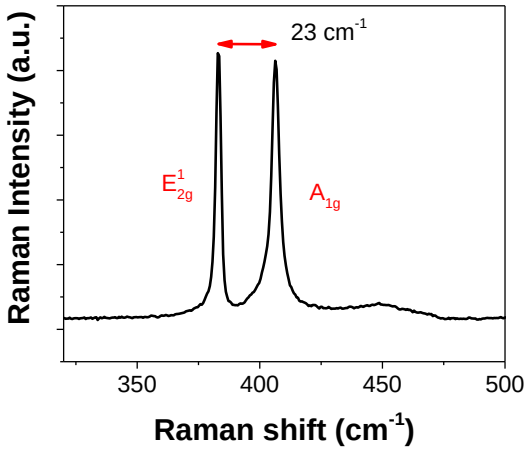

Figure S2. Raman spectrum of MoS_2. The difference between E_{2g}^1 and A_{1g} Raman modes is about 23 cm^{-1}, indicating the sample is bilayer MoS_2.

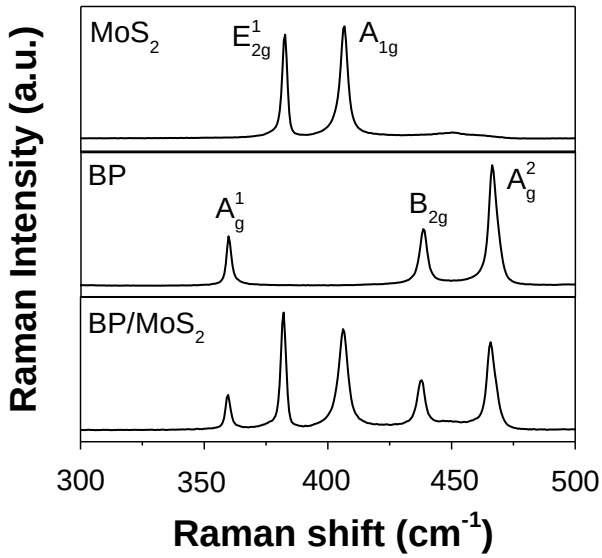

Figure S3. Raman spectra of MoS_2, BP and the BP/MoS_2 heterostructure.

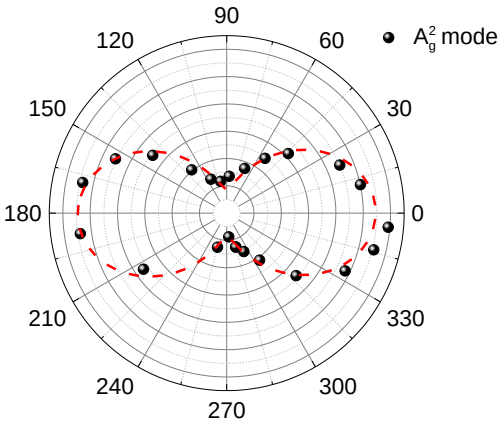

Figure S4. Intensity of the A_g^2 mode of BP film as a function of the excitation laser polarization angle. The dashed red line shows the fitting of data and the maximum corresponds to 0 degree or X direction (armchair direction).

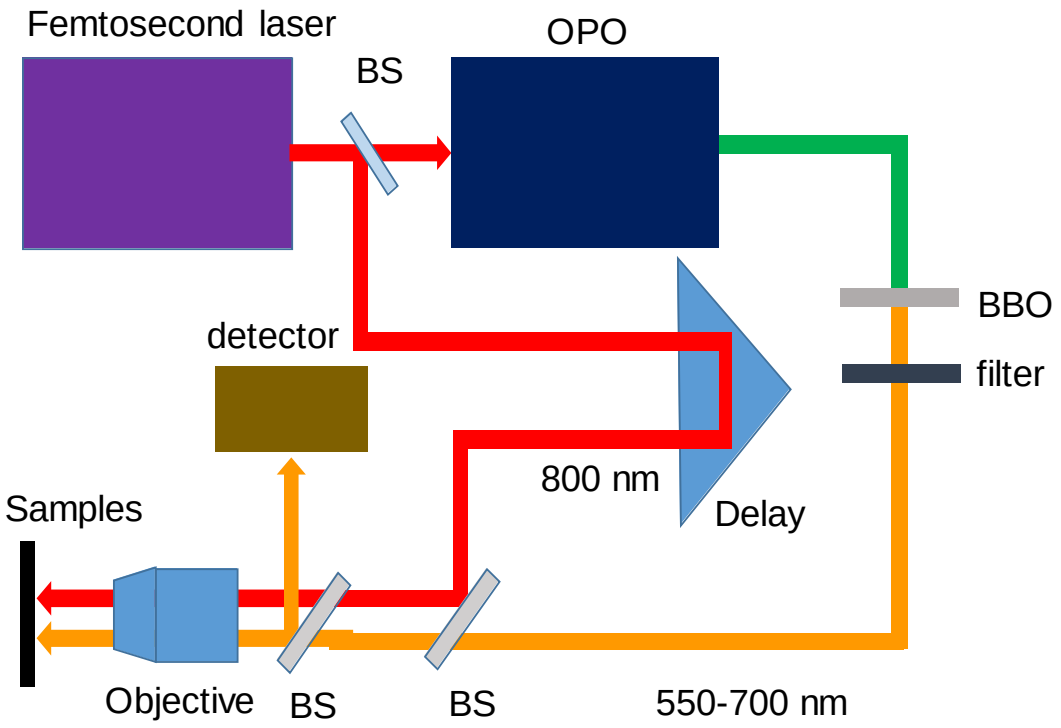

Figure S5. A schematic diagram of the pump-probe setup. OPO: optical parametric oscillator; BBO: Beta barium borate; BS: beam splitter.

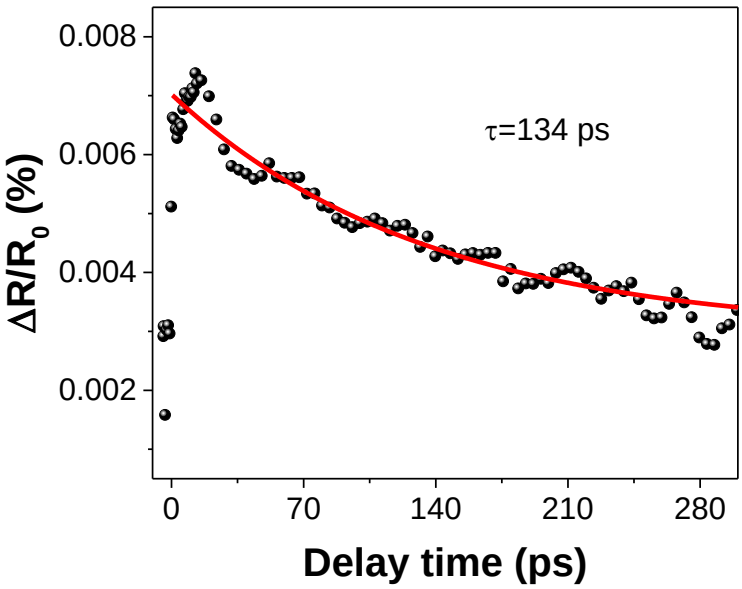

Figure S6. The transient signal from BP film when pump and probe wavelength are 800 nm and 1050 nm respectively.

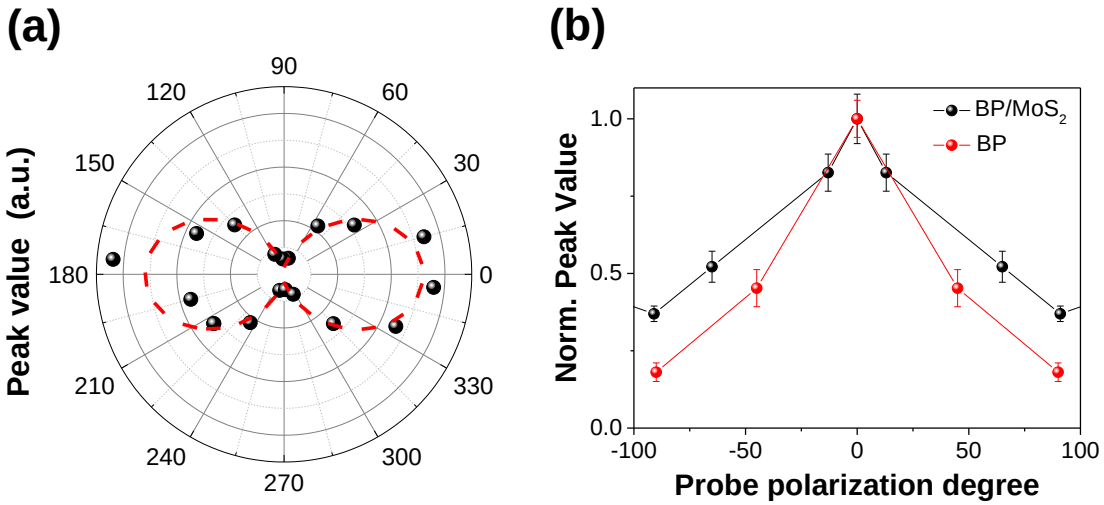

Figure S7. The anisotropic properties of transient photo-response of the heterostructure. (a) Transient signal peak values of the heterostructure under different pump polarization, when pump and probe wavelength are 800 nm and 620 nm respectively. (b) Normalized transient signal peak values of individual BP film and the heterostructure as functions of probe polarization from -100 to 100 degree, when pump polarization is fixed at 0 degree.

Supplementary Note 1: Pump-probe setup

A customized pump-probe setup has been constructed to perform the measurements, shown in Fig. S4. In this setup, a 76 MHz mode-locked Ti: sapphire laser generates 100 fs pulses with a central wavelength in the range of 740-900 nm. A beam splitter separates the laser into two parts. The major part (~80%) of the laser is used to pump a commercial optical parametric oscillator (OPO) to obtain tunable pulses from 1000 nm to 3000 nm, which are focused onto a beta barium borate (BBO) crystal to generate second harmonic generation (SHG) beam to work as probe. The other part of laser goes through the delay stage and works as pump beam to excite photocarriers into the BP layer of the heterostructure. By adopting an 80X microscope objective, the pump and probe beams are tightly focused onto the surface of the sample with a diameter of ~ 2 μm, much smaller than the dimension of the sample. For certain measurement, the pump beam with longer wavelength injects hot electron-hole pairs into samples and these hot carriers are monitored by measuring the differential signal of the probe beam with shorter wavelength, while the pump beam is blocked by a suitable filter.

Supplementary Note 2: Langevin recombination model

The Langevin recombination model, conceptually shown in Fig. 3(a), is used to describe the probability for electrons and holes meeting in real space, which is commonly applicable for bulk photovoltaic materials.[1] According to this model, the

rate of change in photocarrier density can be expressed by the equation shown in the manuscript. Assuming that the intrinsic carrier densities in MoS_2 and BP are close,[2,3] a simplified solution can be obtained:

$$\Delta \mathrm{n(t)} = [(\Delta n(0) + n_0)^{-s} - sBt]^{-\frac{1}{s}} - n_0 \qquad S(1)$$

where Δn is the photocarrier density, n_0 (p_0) is the intrinsic carrier density in MoS_2 (BP), and $\Delta n(0)$ is the initial photocarrier density. As is shown by Fig. 3(b), the transient reflection curves at different pump fluences can be well fitted by Equation S(1) when s=1.2 is adopted. The fitted values of intrinsic carrier density in the two constituent materials and the Langevin recombination constant are listed in Table S1.

Table S1. The parameters obtained by fitting the transient reflection signals to Equation S(1).

Parameter	Fitted value
n_0 (p_0)	(4.9±0.5) ×10^{12} cm^{-2}
B	(2.33±0.25) ×10^{-10} m^2/s

The fitted intrinsic carrier densities in MoS_2 and BP are on the same order of magnitude as the previously reported values.[2,3] Besides the carrier density, another key parameter, the Langevin recombination constant B, is fitted to be ~ (2.33±0.25)×10^{-10} m^2/s, much larger than what was estimated for an all-TMD based heterostructure (~ 4×10^{-13} m^2/s when s=1.2).[3] According to the Langevin model,[1] the constant B is linked to several fundamental parameters and can be written as

$$B = \frac{3\sqrt{\pi}}{4} \frac{e\,(\mu_n + \mu_p)}{\varepsilon\,\varepsilon_0}\, l^{3/2} \qquad \text{S(2)}$$

where μ_n and μ_p are carriers' mobilities in the *n*-type and *p*-type materials respectively, *l* is the space distance between the two materials in the heterostructure, *e* is electron charge, and ε (ε_0) is relative (vacuum) permittivity. From Equation S(2), it should be noted that the Langevin constant *B* is proportional to carrier mobility. As the hole mobility in BP is much larger than that of TMDs,[4] the sum of electron and hole mobility in BP/MoS_2 should be significantly higher than those of TMD heterostructures, which could be responsible for the much larger Langevin recombination constant *B* in our case.

Supplementary Note 3: Anisotropic dynamics of BP/MoS_2 heterostructure

Due to the presence of the BP film, the anisotropic property should be a key feature of the BP/MoS_2 heterostructure and can provide a new degree of freedom for tuning the light-matter interaction in BP-based heterostructure devices.[5,6] Pump-probe measurements were performed with the polarization angle of the pump beam (800 nm) being varied and that of the probe beam (620 nm) being fixed. Peak values of the transient differential reflection of the heterostructure under different pump polarization have been summarized in Fig. S7(a) and the dashed red line shows the fitting result. The anisotropy of the heterostructure is consistent with that of the individual BP film, where the peak value reaches the maximum when the polarization of the pump beam aligns to zero degree, *i.e.*, the armchair direction.[5-7] It

indicates that the transferred photo-generated electrons still conserve the same anisotropy inherited from the BP film to a considerable extent. The BP/MoS_2 heterostructure therefore could be applied for the polarization-sensitive devices. To further reveal the difference between anisotropic property of the BP/MoS_2 heterostructure and that of the pure BP film, we performed measurements by fixing the polarization of the pump beam (800 nm) (*i.e.*, the photocarriers' anisotropic distribution at the initial stage) and varying that of the probe beam (620 nm). The polarization-dependent transient reflection peak values of the heterostructure are shown in Fig. S7(b) by the black dots. For comparison, the transient spectroscopy on pure BP film (pump ~800 nm, probe ~1050 nm) has been performed in the same way, the signal of which is shown by the red dots in Fig. S7(b). It is apparent that the anisotropy of the heterostructure has been weakened compared with that of the individual BP film. The reduction of anisotropy is likely as a result of the isotropic symmetry of MoS_2, *i.e*., the isotropic redistribution after the electron transfer process.

References

1 G. Juška, K. Genevičius, N. Nekrašas, G. Sliaužys and R. Österbacka, *Appl. Phys. Lett.* 2009, **95**, 013303.

2 S. Ge, C. Li, Z. Zhang, C. Zhang, Y. Zhang, J. Qiu, Q. Wang, J. Liu, S. Jia, J. Feng and D. Sun, *Nano Lett.* 2015, **15**, 4650-4656.

3 C. H. Lee, G. H. Lee, A. M. van der Zande, W. Chen, Y. Li, M. Han, X. Cui, G. Arefe, C. Nuckolls, T. F. Heinz, J. Guo, J. Hone and P. Kim, *Nat. Nanotechnol.* 2014, **9**, 676-681.

4 F. Xia, H. Wang and Y. Jia, *Nat. Commun.* 2014, **5**, 4458.

5 L. Li, Y. Yu, G. J. Ye, Q. Ge, X. Ou, H. Wu, D. Feng, X. H. Chen and Y. Zhang, *Nat.*

Nanotechnol. 2014, **9**, 372-377.
6 L. Li, J. Kim, C. Jin, G. J. Ye, D. Y. Qiu, F. H. da Jornada, Z. Shi, L. Chen, Z. Zhang, F. Yang, K. Watanabe, T. Taniguchi, W. Ren, S. G. Louie, X. H. Chen, Y. Zhang and F. Wang, *Nat. Nanotechnol.* 2017, **12**, 21-25.
7 H. Yuan, X. Liu, F. Afshinmanesh, W. Li, G. Xu, J. Sun, B. Lian, A. G. Curto, G. Ye, Y. Hikita, Z. Shen, S. C. Zhang, X. Chen, M. Brongersma, H. Y. Hwang and Y. Cui, *Nat. Nanotechnol.* 2015, **10**, 707-713.